Towards Quantum Computation with Single Fermionic Atoms in Micro-Optical Traps

Ph.D research proposal by Yanay Florshaim

Advisor: Prof. Yoav Sagi

May 31, 2018

Department of Physics

Technion - Israel Institute of Technology, Haifa, Israel

Abstract

This research proposal implements a new method of a two-qubit gate in a ultracold fermionic system. This method is based on the experimental toolbox in ultracold atom apparatus and the fermionic statistic. In addition, this work presents a $\sqrt{\text{SWAP}}$ gate protocol that gives such systems the ability to break the technology limit of a quantum computer of this days. As I describe in this proposal, the new platform based on ultracold ^{40}K fermionic atom held in an optical microtraps. The quantum information can be stored in the internal states of these atoms or in vibrational states of the trap. The universal two-qubit $\sqrt{\text{SWAP}}$ gate can be implemented by a novel protocol that takes advantage of the ability to precisely control the tunneling energy and the interaction energy (by using Feshbach resonance) between two atoms at two adjacent traps. Then, this work presents our new apparatus design and describes the open questions for this research.

Contents

1 Introduction

This chapter provides a short introduction to ultracold atomic systems and then explains the motivation and requirements for quantum computation.

1.1 Ultracold atoms

Ultracold atomic gases allow exceptional purity in preparing a state almost completely isolated from the surrounding, and offer unparalleled experimental control. It is possible to prepare the atoms in a well-defined internal state, and to cool the external motion almost to the ground state. The cooling methods can be divided into two types. First, a laser close to resonance is used to cool the atoms to approximately 10 μK in ^{40}K. Second, the atoms are held in a conservative potential (magnetic or optical) and only the hottest atoms are removed, a process call forced evaporation. One of the important tools in such systems is the ability to tune the interactions from repulsive to attractive, and from weak to strong. This is done by applying a uniform magnetic field close to a Fano-Feshbach resonance.

1.1.1 Feshbach resonance in cold atoms

In the vicinity of a Feshbach resonance, the strength of interaction can be widely tuned, and is described by a single parameter, the s-wave scattering length, defined by

$$a = -\lim_{k \ll 1/r_0} \frac{\tan(\delta_0)}{k} \quad , \tag{1}$$

where k is the scattered atom momentum, r_0 is the interaction range, and δ_0 is the phase shift between the incoming and the scattered wave-functions. For alkali atoms (such as ^{40}K), the scattering length is around the van der Waals atomic range $a \sim r_0 = 50 - 100a_0$, where a_0 is the Bohr radius. In this case, $k_F a \approx 0.03 \ll 1$, which means that the gas is weakly interacting gas. Note that we have compared the scattering length to the k_F which gives the natural units of length to the problem. The scattering length can be tuned from negative to positive, making the atoms vary from attractive to repulsive, respectively.

The key to manipulating the scattering length stems from the coupling between molecular states with different total magnetic moments, namely the singlet and triplet states. The triplet channel is referred to as an open channel and the singlet state is referred to as an close channel. The relative Zeeman shifts between these two channels can be used to tune the energy of the high bound state of the open channel into resonance with the energy of the incoming atoms. As a result, the scattering length diverges at the resonance and its

dependence on the magnetic field is given by:

$$a(B) = a_{bg}\left(1 - \frac{\Delta B}{B - B_0}\right) \tag{2}$$

where a_{bg} is the background scattering length away from resonance, ΔB is the resonance width, and B_0 is the resonance position. In ^{40}K, the parameters for the Feshbach resonance between the states $|F = 9/2, m_f = -9/2\rangle$ and $|F = 9/2, m_f = -7/2\rangle$ are: $a_{bg} = 169.7\, a_0$, $B_0 = 202.14\,(1)$ G, $\Delta B = 6.70\,(3)$ G [33]. These parameters were obtained using a new high sensitivity rf spectroscopy method we have developed in the group, and is part of the preliminary results described in section 3.2. There are other resonances between different spin states, however these states are not immune to detrimental spin-exchange collisions. In our proposed quantum computation platform, Fechbach resonance will be used to control the on-site interaction, and will therefore be important in the implementation of the two qubit gate.

1.1.2 Optical dipole trap

Another powerful experimental tool is the ability to trap and manipulate atoms in a far-off-resonance laser beam. This section introduces the mechanism of optical trapping in cold atomic systems.

When an electric field $\vec{E}$ oscillating with a frequency ω, such as the light field, acts on a neutral atom, it induces an electric dipole moment

$$p = \alpha E \quad , \tag{3}$$

where α is the complex polarizability. This electric dipole moment interacts with the light field yielding the following potential energy:

$$U_{dip} = -\frac{1}{2}\langle pE\rangle \propto -\mathrm{Re}(\alpha)\,|E|^2 \tag{4}$$

Therefore, the potential energy is proportional to the intensity $I \propto |E|^2$ of the oscillating field. The full expression for the dipole potential is given by [15]:

$$U_{dip}(r) = \frac{3\pi c^2 \Gamma}{2\hbar\omega_{0,1}^3 \delta} I(r) \tag{5}$$

where $I(r)$ is the laser beam intensity, Γ is the natural line-width, and $\delta = \omega - \omega_{0,1}$ is the frequency detuning of the laser from the frequency of the optical transition $\omega_{0,1}$. The dipole trap can be attractive for red detuning ($\delta < 0$) or repulsive for blue detuning ($\delta > 0$). For

a TEM_{00} Gaussian mode, the potential near the trap minimum can be expanded to second order in position as:

$$U_{dip}(r,z) = -U_0\left[1 - 2\left(r/\omega_0\right)^2 - \left(z/z_R\right)^2\right] \tag{6}$$

where ω_0 is the beam waist, z_r is the Rayleigh range, and U_0 is the trap depth. The corresponding harmonic oscillator frequencies are $\omega_r = \sqrt{\frac{4U_0}{m\omega_0^2}}$ and $\omega_z = \sqrt{\frac{2U_0}{mz_R^2}}$ for the radial and axial directions, respectively. In addition to a conservative potential, the interaction with the light beam leads to spontaneous emission which is irreversible and causes heating. The rate of this scattering is given by:

$$\Gamma_{sc} = \frac{\Gamma}{\hbar\delta}U_{dip} \quad . \tag{7}$$

From this equation it is clear that for a given potential depth, it is advantagous to work at higher detuning which minimizes the scattering rate. For this reason for quantum computation and quantum simulation we will use a laser which is far-off resonance $\delta \gg \Gamma$.

1.2 Quantum computation and simulation

In quantum mechanics, the dimension of the Hilbert space grows exponentially with the system size. In order to represent a quantum state with n particles in classical computation we need an order of C^n bytes, where C is a constant. Therefore, it is practically impossible to calculate a many-body quantum state (e.g. ground state of a given Hamiltonian) with a classical computer. To overcome this problem, Richard Feynman first proposed to use a quantum computational machine ("Quantum Computer")[14]. A quantum computer takes advantage of quantum coherence and superposition and can therefore simulate quantum dynamics and solve exponentially faster complex mathematical problems. For more than two decades, researchers have been trying to implement quantum computation using different platforms, including optics [26], ion traps [9, 17], quantum dots [19], neutral atoms in optic trap [35], and superconductivity devices [2]. These platforms have made considerable progress, but none of them has become scalable and technologically fully feasible. Therefore, there is still a motivation to explore alternative platforms, such as the one presented in this proposal.

For a system to be a quantum computer it has to meet certain requirements, as first formulated by D.DiVincenzo [11]:

- **Having a well-defined quantum state.** The quantum state is where quantum information in encoded in a quantum computer, and it needs to be well-defined. In quantum computation two states are usually enough for this encoding ("qubit"): $|0\rangle$ and $|1\rangle$. The qubit state is given by

$$|\psi\rangle = \alpha\,|0\rangle + \beta\,|1\rangle \quad , \tag{8}$$

where α and β are complex numbers. When the qubit is measured, the probability of it being in state $|0\rangle$ or $|1\rangle$ is given by $|\alpha|^2$ and $|\beta|^2$, respectively. The normalization of the state ensures: $|\alpha|^2 + |\beta|^2 = 1$.

- **Preparation of the initial state.** The system should allow initialization of of the qubit state. The initial state is of little importance as we can manipulate it later with quantum gates, thus reaching any other desired state.

- **Quantum gates.** It should be possible implement a set of universal unitary operators ("Quantum Gates"). These gates act either on a single qubit or on two qubits. There are several types of one-qubit gates such as a Hadamard gate, a phase gate, and a $\pi/8$ gate. One possible choice for a universal two-qubit gate is the quantum C-NOT gate. $\sqrt{\text{SWAP}}$ gate is another universal two-qubit gate [23]. By taking a specific cumulative series of these gates, any other unitary operation on n qubits can be constructed [25].

- **Ability to measure the result.** The ability to measure the final state of the system is required for all computation systems. In particular, the detection method needs to confirm the qubit still exist and was not lost during the computation process. In addition, it should be able to measure the qubit state.

- **System scalability.** The physical resources (e.g., space and money) should not scale as X^n, where X is some system constant and n is the number of qubits. In addition, detrimental effects per qubit, such as decoherence or loss, should not grow with the system size.

Another issue that exists in the real world is decoherence due to undesirable interactions between the quantum computer and its environment. Therefore, the time-scale T_1 during which the system is isolated from the environment must be smaller than the preparation time of all the operation T_{gate}.

$$\frac{T_{gate}}{T_1} \ll 1 \tag{9}$$

In our proposed platform the calculated ratio is $\frac{T_{gate}}{T_1} \sim 10^{-5}$ which is promising.

2 A new platform of quantum computation

This chapter describes how the five conditions for quantum computation can be realized in the proposed computational scheme using single fermionic atoms in micro-optical traps. The $\sqrt{\text{SWAP}}$ gate was developed by Dr. Jonathan Nemirovsky.

2.1 The qubit

The proposed quantum computer is based on two internal energy levels of a ^{40}K atom held in a microtrap. During the gate operation the qubit will be encoded in the states $|\downarrow\rangle = |0, 9/2, -9/2\rangle$ and $|\uparrow\rangle = |0, 9/2, -7/2\rangle$ with notation $|n, F, m_f\rangle$, where n is the vibrational state, F is the total atomic spin, and m_f is the projection in $\hat{z}$ direction (set by external magnetic field). The interaction between these states can be controlled by means of a Feshbach resonance around $B = 202.14$ G, and this tunability is important for implementing the two-qubit gate (for more detail see section 2.3). However, the energy difference between these states is sensitive to magnetic field fluctuations, hence a qubit encoded in these states for long durations may suffer from fast decoherence. It is possible to transfer the encoding in-between operation to other states which are more resilient to magnetic noise. Two options for that are magnetic insensitive states ("clock transition") or encoding in different vibrational states but with the same magnetic moment. A more complicated option we may later consider is using two physical qubits to encode one logical qubit, and encoding the information in a decoherence subspace of these two qubits. such a solution, however, will require generalization of the qubit operations described later.

2.2 Preparation of the initial state

The requirement is to prepare a single atom in the ground state of a micro optical trap at a specific spin state. It is important that the initial state can be created with high fidelity. There are two routes to achieve this. One option is to prepare first a quantum degenerate Fermi gas in a single spin and load directly from it a microtrap, then reduce the microtrap depth until only a single atom at the ground state is left. As was shown by S. Jochim's group, this process can be engineered to achieve a single fermionic atom at the ground state at very high fidelity [31]. A different route is to cool inside the trap in a process that will make sure we are left with only a single atoms at the ground state. Having a single atom is usually guaranteed as a result of light assisted collisions which remove atoms until only a single one is left in the trap. A cooling process such as Raman side-band cooling can be used to cool in trap and at the same time optically pump the atom to a desired spin state. However, optical cooling of single fermionic atom in trap has not yet been demonstrated. The advantage of the second route is that the preparation time is expected to be considerably shorted than at the first route. More details will be given in the section describing the experimental system section 4.1.

2.3 Quantum gates

As mentioned before, to implement a quantum computer, a single-qubit **Hadamard gate**, **phase gate**, **$\pi/8$ gate**, and the two-qubit gate $\sqrt{\text{SWAP}}$ **gate** should be realized in our

system:

2.3.1 Single qubit gate

Any unitary transformation on a single qubit can be decomposed into rotations in the Bloch sphere around some axis $\hat{n}$ by an angle θ multiplied by a global phase ϕ

$$U = e^{i\phi} e^{-i\frac{\theta}{2}\cdot\hat{\sigma}_n} \quad ,$$

where $\hat{\sigma}_n$ is Pauli matrices. This unitary transformation can be realized in an ultracold atomic system by coupling the two levels of the qubit to an external electromagnetic field [1, 20]. This is usually done by rf radiation. The experimental parameters that control the Bloch sphere rotation are the phase of the rf pulse and the detuning between its frequency and the two different energy states divided by $\hbar$. Single qubit operation in general relatively simple to implement. However, the challenging aspect is to perform these operations only on one of the qubits, sometimes referred to as "addressing" the qubit. We consider several options for addressing, including using Raman transitions with laser beams instead of rf (which in comparison has very long wavelength) or shuttling the atoms to a particular position where the single qubit operations can be done without affecting the other qubits.

2.3.2 Two qubit $\sqrt{\text{SWAP}}$ gate

The $\sqrt{\text{SWAP}}$ is a two-qubit gate that swaps the states half-way, namely when applied twice it will swap the qubits. It can written explicitly with respect to the basis $|\downarrow\downarrow\rangle$, $|\downarrow\uparrow\rangle$, $|\uparrow\downarrow\rangle$, $|\uparrow\uparrow\rangle$ as:

$$U_{\sqrt{swap}} = \begin{bmatrix} 1 & 0 & 0 & 0 \\ 0 & \frac{1}{2}(1+i) & \frac{1}{2}(1-i) & 0 \\ 0 & \frac{1}{2}(1-i) & \frac{1}{2}(1+i) & 0 \\ 0 & 0 & 0 & 1 \end{bmatrix} \quad . \tag{10}$$

In Bell state representation, the $\sqrt{\text{SWAP}}$ only changes the anti-symmetric state to

$$\left(\hat{d_1}^{\dagger}\hat{u_2}^{\dagger} - \hat{u_1}^{\dagger}\hat{d_2}^{\dagger}\right)|\psi\rangle \rightarrow i\left(\hat{d_1}^{\dagger}\hat{u_2}^{\dagger} - \hat{u_1}^{\dagger}\hat{d_2}^{\dagger}\right)|\psi\rangle \quad , \tag{11}$$

while other states are unchanged. Our protocol is original but similar in some aspects to the gate first described in Ref. [16]. The system includes two optical microtraps with a single atom at each site with a distance $d(t)$ between them. Using second quantization formalism and the Fermi-Hubbard model [18], the Hamiltonian is given by

$$H_{J,U} = J \cdot \left(\hat{u}_1^{\dagger}\hat{u}_2 + \hat{u}_2^{\dagger}\hat{u}_1 + \hat{d}_1^{\dagger}\hat{d}_2 + \hat{d}_2^{\dagger}\hat{d}_1\right) + 2U \cdot \left(\hat{u}_1^{\dagger}\hat{u}_1\hat{d}_1^{\dagger}\hat{d}_1 + \hat{u}_2^{\dagger}\hat{u}_2\hat{d}_2^{\dagger}\hat{d}_2\right) \tag{12}$$

$$\equiv J \cdot H_J + U \cdot H_u \tag{13}$$

Where J is the tunnelling energy, U is on site interaction energy, $\hat{u}_i$ and $\hat{u}_i^\dagger$ are annihilation and creation operators of particle i in state $|\uparrow\rangle$, and $\hat{d}_i$ and $\hat{d}_i^\dagger$ are annihilation and creation operators of particle i in state $|\downarrow\rangle$. By tunning the system parameters $U = U_1$ with Feshbach resonance and $J = J_1$ with the distance between the qubits $d(t)$ and set the gate duration as T_1, the dynamics of the Hamiltonian are given by

$$\sqrt{\text{SWAP}} = \exp\left(-iT_1 H(U_1, J_1)/\hbar\right)$$

The conditions on U_1 and T_1 are:

$$U_1 = \pm\frac{2J\hbar\left(2n-\frac{1}{2}\right)}{\sqrt{m^2-\left(2n-\frac{1}{2}\right)^2}} \qquad\qquad T_1 = \frac{\hbar\pi\sqrt{m^2-\left(2n-\frac{1}{2}\right)^2}}{2J} \tag{14}$$

Where m is an odd integer and n is any integer. The last parameter, J_1, depends on the distance between the two-qubits, i.e., $d(t)$.
The $\sqrt{\text{SWAP}}$ gate can be realized in the following stages.

1. The tunneling was set to some value $J = J_1$ and the interaction was determined to be $U = 0$. Then, after $t_1 = \frac{\pi\hbar}{4J_1}$, the dynamic for the anti-symmetric state $|\psi_A\rangle$ state was obtained.
$$\left(\hat{d_1}^\dagger\hat{u_2}^\dagger - \hat{u_1}^\dagger\hat{d_2}^\dagger\right)|0\rangle \rightarrow -i\left(\hat{d_1}^\dagger\hat{u_1}^\dagger + \hat{u_2}^\dagger\hat{d_2}^\dagger\right)|0\rangle . \tag{15}$$
while the symmetric states $\hat{d_1}^\dagger\hat{u_2}^\dagger + \hat{u_1}^\dagger\hat{d_2}^\dagger$, $\hat{u_1}^\dagger\hat{u_2}^\dagger$, $\hat{d_1}^\dagger\hat{d_2}^\dagger$ are stationary, due to Pauli exclusion principle.

2. The tunneling energy was set to zero, $J = 0$ and the interaction $U = U_1$ for a duration of $t_2 = \frac{\pi\hbar}{4U_1}$. As a result, the symmetric states do not change when the $|\psi_A\rangle$ state is now
$$-i\left(\hat{d_1}^\dagger\hat{u_1}^\dagger + \hat{u_2}^\dagger\hat{d_2}^\dagger\right)|0\rangle \rightarrow -\left(\hat{d_1}^\dagger\hat{u_1}^\dagger + \hat{u_2}^\dagger\hat{d_2}^\dagger\right)|0\rangle \tag{16}$$

3. The last stage repeats the first stage by setting the tunneling energy as $J = J_1$ and turns off the interaction. The waiting time was $t_1 = \frac{\pi\hbar}{4J_1}$, and the symmetric state, again, did not change while the anti-symmetric state returned to the original state $|\psi_A\rangle$ with a phase of $e^{i\pi/2}$
$$-\left(\hat{d_1}^\dagger\hat{u_1}^\dagger + \hat{u_2}^\dagger\hat{d_2}^\dagger\right)|0\rangle \rightarrow i\left(\hat{d_1}^\dagger\hat{u_2}^\dagger - \hat{u_1}^\dagger\hat{d_2}^\dagger\right)|0\rangle \tag{17}$$
which gives the $\sqrt{\text{SWAP}}$ gate.

The gate duration $\tau = 2t_1 + t_2$, is proportional to U^{-1} and J^{-1}. The parameter U controlled by an external magnetic field, while the J is determined by the overlap between the wave functions in the two traps, and it can be calculated by the difference between the symmetric and the anti-symmetric energies. A 3D numerical calculation of two Gaussian double wells was used to evaluate the $\sqrt{\text{SWAP}}$ gate duration $T_{\sqrt{SWAP}}$ vs. the numerical aperture (NA) of the objective generating the micro traps. The NA determines all the properties of the microtraps. As shown in figure 1, the tunnelling time increases exponentially for lower NA. Therefore, a high NA is needed for the $\sqrt{\text{SWAP}}$ gate. For NA larger than 0.7 the gate time can be few milliseconds, which is 5 orders of magnitude smaller than a typical vacuum lifetime, which sets the time-scale T_1.

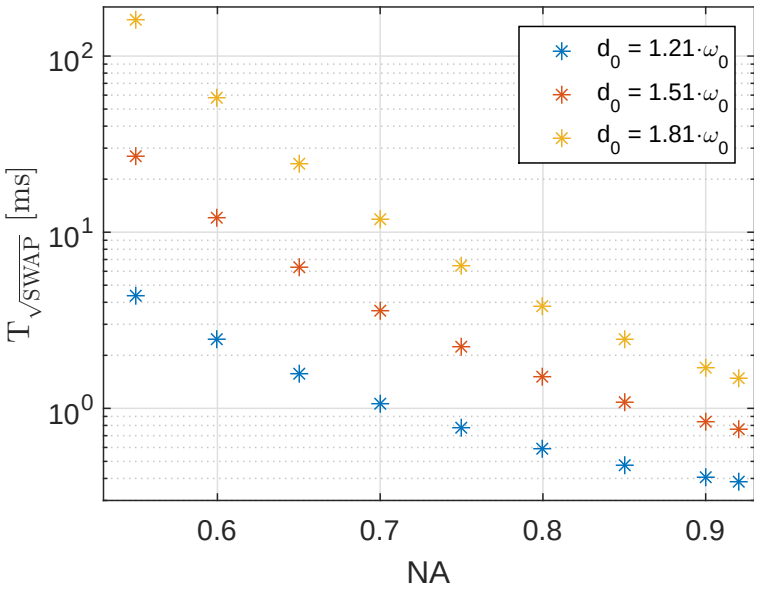

Figure 1 – Calculation of gate duration $T_{\sqrt{\text{SWAP}}}$ vs. NA for a given distance x_0. In this calculation, the wavelength is $\lambda = 1064$ nm, and the depth of each of the traps is $V_0/k_b = 310$nK.

2.4 Detection

After qubit initialization and applying the series of quantum gates, the final state of each qubit needs to be reliably detected. A detection of a single atom by is by itself a challenging task, and discerning its state makes it even more so. To detect a single atom the common approach is to scatter enough photons from it (fluorescence imaging). However, a single ^{40}K atom cannot be detected inside the optical trap with fluorescence imaging on the cycling transition $|-9/2,-9/2\rangle_{^2S_{1/2}} \longrightarrow |11/2,-11/2\rangle_{^2P_{3/2}}$ due to the $3D_{3/2}$ transition which is

detuned 1169nm from the $^2P_{3/2}$ state [8]. Several groups have coped with this problem in recent years in the context of quantum gas microscopes, and they developed new techniques to detect a single ^{40}K atom. In section 4.3, we discuss the three alternative methods.

2.5 Scalability

Scalability in our scheme is fairly straightforward. The cooling sequence is the same for many qubits only requiring the generation of many microtrap and loading them in parallel [3]. A convenient method to create several microtraps is to generate beams at different angles and then the objective translate their angle to different position in the focal plane, which is where the microtrap are generated. The position of a beam coming at an angle theta is simply given by $\theta = f \cdot d$ Where d is the distance between two microtraps and f is the objective focal length. One way to control dynamically the relative angle θ is to use Acousto-Optic-Deflector (AOD). By placing two AOD in an orthogonal direction, the position of the microtraps in the focal plane plane can be moved in two dimensions [21].

3 Preliminary results

Over the past three years, I had an important role in the construction of the first apparatus in the group of Prof. Yoav Sagi. I have spent time testing some of the methods we are going to incorporate in the new setup. All the preliminary results discussed here were obtained with the first apparatus.

This apparatus is composed of three chambers under ultrahigh vacuum (see figure 2). In the first chamber (source), ^{40}K atoms are released from home-made dispensers and immediately captured by a 2D Magneto optical trap (MOT). On the third axis, there is a mirror with a hole (nozzle) inside the chamber. The atoms are cooled in two axes and then pushed to the second chamber by another laser throw the nozzle. In the second chamber (cooling), the atoms are captured by a 3D MOT. At this point, the atoms cloud temperature is around 220 μK. By using a gray molasses cooling on the D_1 transition, the atomic cloud temperature is reduced to approximately 15 μK. Next, the atoms are optically pumped into the states $|F = 9/2, m_f = 9/2\rangle$ and $|F = 9/2, m_f = 7/2\rangle$ and loaded into a QUIC magnetic trap. In this configuration, the magnetic trap minimum is greater than zero which is important for RF evaporation. Following the evaporation, the temperature is $T/T_f \approx 4.5$ where T_f is the Fermi temperature. Next, the atoms are loaded into a far-off-resonance optical trap that focuses to 39.5 μm with a power of 6 W. The optical trap is moved adiabatically by an air-bearing stage to the science chamber, which is distance of 320 mm. During the movement, the trap waist drops to 19.5 μm and increases the trap depth. Therefore,the laser beam power is lowered in the movement. In the science chamber, a second beam crosses the first beam at an angle of 45° with $\omega_0 = 200\,\mu$m and power of 2.8 W. Finally, the optical evaporation continues to 10 mW in the main beam and 1.5 W in the cross beam. The conditions at the end of the preparation process are ∼150,000 atom per spin state at $T/T_F \approx 0.2$.

3.1 Creating and loading a micro trap

In order to learn about the preparation process described before, we constructed an objective with NA=0.3 and loaded it directly from a quantum degenerate Fermi gas. The objective was designed by us for the existing apparatus.

3.1.1 Home-made objective with NA=0.3

We have simulated geometrical optics effects in commercial available lenses and designed a diffraction limited objective with NA= 0.3 at $\lambda = 1064$ nm. Our design is detailed in table 1 and the simulation is shown in figure 3a. We have also designed and manufactured a holder from Ultem with spacers made of aluminium. This design was made to ensure accurate distances between the elements using metallic spacers, but allowing their removal later to

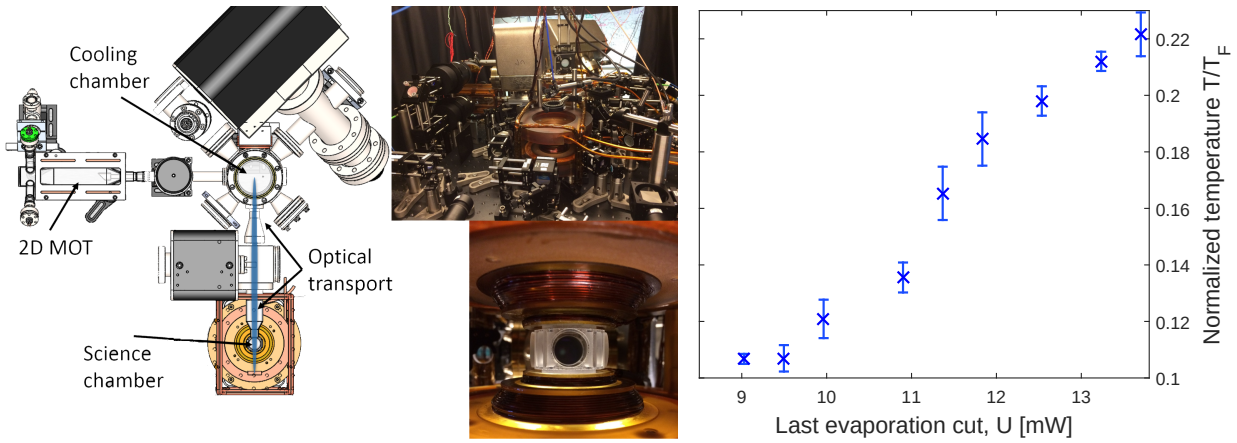

(a) **(b)**

Figure 2 – (a) Top view of the existing experimental apparatus. (b) The final temperature normalized to the Fermi temperature, T/T_F, vs. optical trap power during the final evaporation. Quantum degeneracy of $T/T_F \sim 0.1$ is achieved.

prevent eddy currents.

The objective was characterized by two independent measurements. First, a waist of $\omega_0 = 2.35\,\mu$m was measured using a knife edge technique. This measurement had a spatial resolution of ~ 50 nm using a Michelson interferometer as a calibration for the distance (see figure 4a). Second, by imaging a 1951 USAF resolution target, a resolution of 4.4 μm was obtained. The point spread function (PSF) was directly measured by imaging a pinhole of 1 μm with diameter tolerance of $+0.25/-0.1\,\mu$m. A NA $= 0.258 \pm 0.03$ was extracted by fitting directly the PSF and NA $= 0.289 \pm 0.0083$ was obtained from the modulation transfer function (MTF) calculation which is the mathematical Fourier transform of the PSF figure 4b. Two objectives were eventually built, and both are now in use in the setup.

3.1.2 Loading a single atom to microtrap

In degenerate Fermi gas, the occupation probability for a state with energy ϵ is $P(\epsilon) = (\exp\left(\frac{\epsilon-\mu}{k_B T}\right) + 1)^{-1}$, where μ is the chemical potential, k_b is a Boltzmann constant, and T is the temperature. We have chosen the trap parameters such that $P(E_0) > 0.999$, where E_0 is the ground state energy. The number of atoms loaded into the microtrap are calculated

Surface number	Catalog number	Radius [mm]	Distance to the next surface [mm]	Material
1	LC1582	∞	3.5	BK7
2	-	38.6	10.92	air
3	LB1901	76.6	4.1	BK7
4		-76.6	10	air
5	LA1608	38.6	4.1	BK7
6		∞	2	air
7	LE1234	32.1	3.6	BK7
8		82.2	21	air
9	Vacuum window	∞	3.15	Silica
10		∞	-	Vacuum

Table 1 – The design of our NA= 0.3 objective (lenses are from Thorlabs).

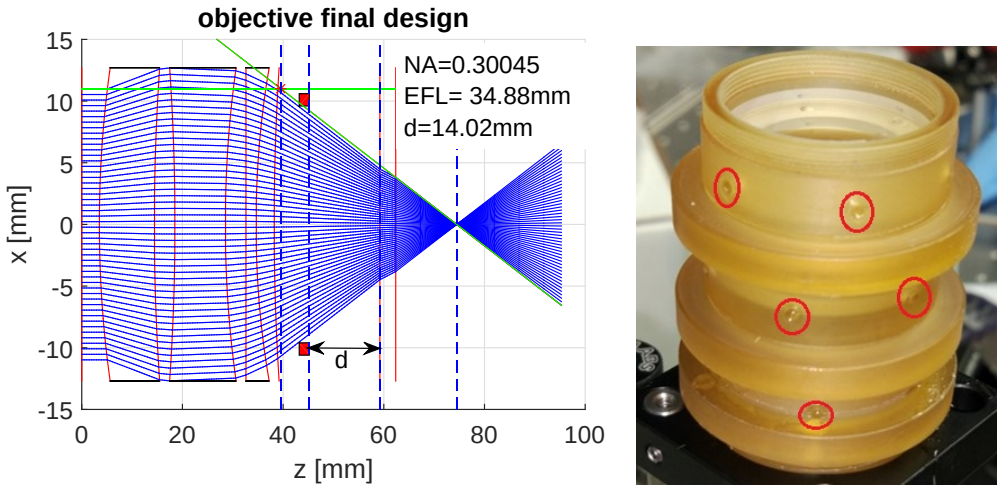

(a) **(b)**

Figure 3 – (a) Computer simulation of the objective's performance (MATLAB). The simulation predicts $NA = 0.3$ and an effective focal length of 34.88 mm, which gives a diffraction limit of $\omega_0 = 1.12$ μm at $\lambda = 1064$ mm. This calculation includes the vacuum window and the distance of the atoms from the window. (b) Image of the objective after assembly. The small holes (red circles) are designed to allow gluing the lenses to the plastic parts and removing the metallic spacers.

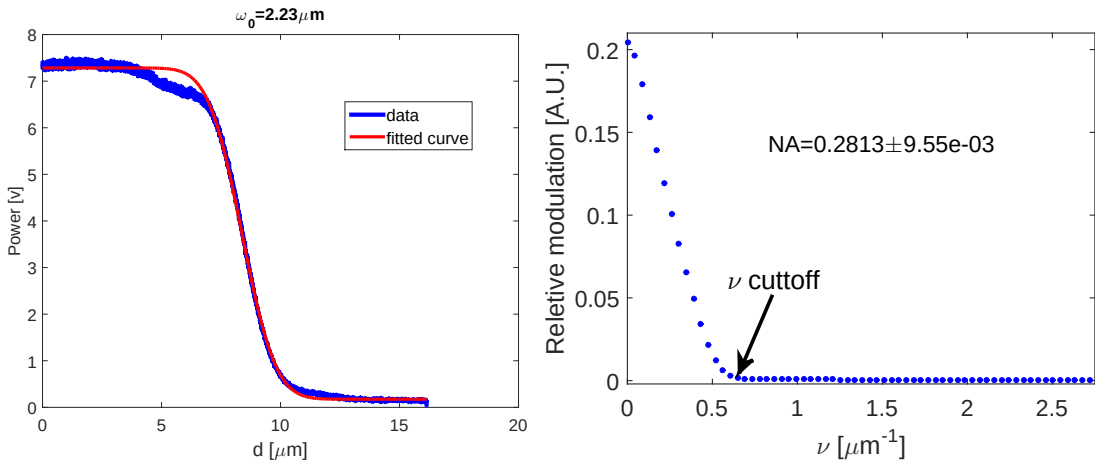

Figure 4 – (a) Measuring the objective NA using knife edge technique (blue is data, red is fit). We calibrate the knife position using a Michelson interferometer. (b) MTF vs. spatial frequency. The cutoff frequency is where the MTF is on the order of the noise.

by counting the number states in the trap:

$$N = \int_0^{U_{max}} P(\epsilon)\, g(\epsilon)\, d\epsilon \quad , \tag{18}$$

where U_{max} is the maximum trap depth and $g(\epsilon)$ is the atoms density of states. In a 3D harmonic potential,the density of states is given by $g(\epsilon) = \frac{\epsilon^2}{2h^3\nu_x\nu_y\nu_z}$ with ν_i being the optical trap oscillation frequency in axis $\hat{i}$. The temperature T and the chemical potential μ, was measured by performing absorption imaging before the microtrap is turned on, and the potential parameters, U_{max} and ν_i were analytically calculated from the potential shape in Eq. 5. For the trap parameters in this work ($\omega_0 = 2.35$), the number of energy states was calculated to be 12 states for power of a 15 μW and 2000 for a power of a 100 μW.

In order to detect small number of atoms, I have built a 3D MOT in the science chamber. Bu comparing the MOT signal to absorption imaging (at large enough atom numbers), I have also calibrated the fluorescence signal. Using the 3D MOT, very small number of atoms could be measured and I proceeded to load the micro-optical trap. To this end, the atomic cloud was prepared with 300,000 atoms per spin state in $T/T_F \approx 0.4$. Then, the microtrap was turned on and approximately 2000 atoms were loaded. Following loading, the dipole trap holding the degenerate cloud was turned off and only the atoms in the micro trap were left.

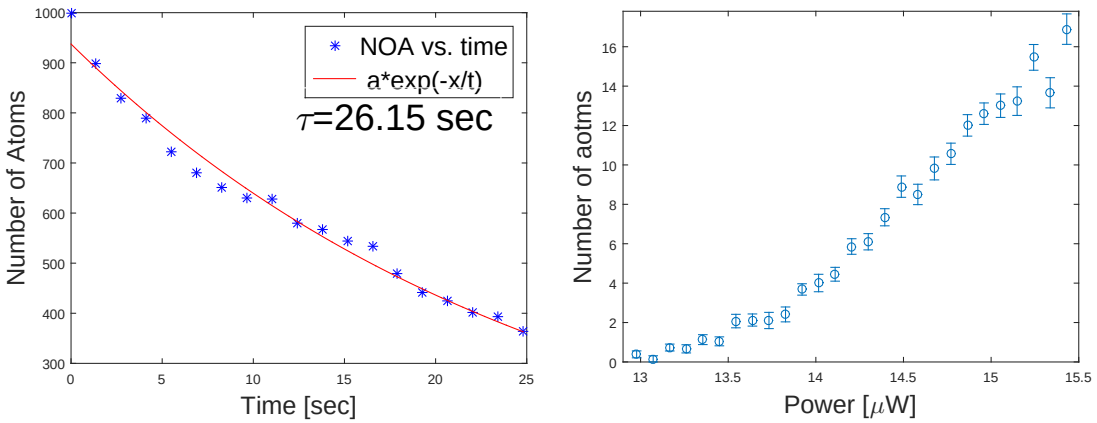

Figure 5 – (a) Measurement of the atoms lifetime in the microtrap. (b) Measurement of the number of atoms vs. laser power. The number of atoms is calculated by taking the camera signal and divided by the calculated signal per atom in our system.

The microtrap laser power was then lowered until $\sim$ 200 atoms were left in the microtrap. Afterwards, the gradient coil was used to apply a gradient of a magnetic field to further decrease the total potential without changing the trapping frequencies. I have measured the lifetime of atoms in the microtrap to be 26sec, as show in figure 5aa. Also, I have measured the number of atoms versus the microtrap laser power, as shown in figure 5b, with a good agreement to the previous calculation and equation 18.

Unfortunately, I have discovered during these experiments that the background of photons scatted by the vacuum chamber windows is very large ($\sim$ 5% per surface), which limited our sensitivity using the 3D MOT to approximately 5 atoms. To overcome this limit, we have purchased and inserted an ultra-narrow band-pass filter that blocks the photons of the D_2 atomic line and only the D_1 photons were transited. In addition, I have added a laser with a wavelength of the D_1 to the 3D MOT optical paths, which initially lowered the signal for the same number of atoms (see figure 6a),but this was amended when a repump was as well. We then obtained almost the same signal as the D_2 3D MOT with a long life time. As shown in figure 6b, these modifications increased the signal to noise (SNR) for exposure time higher from 0.5 sec, and allowed us to reach the single atom sensitivity level.

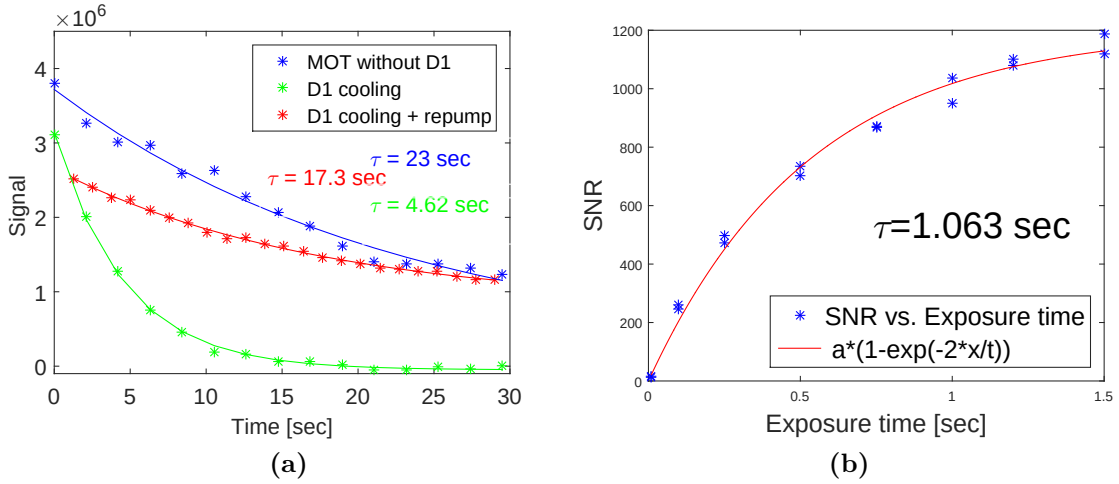

(a) **(b)**

Figure 6 – (a) Lifetime of atoms captured in the science chamber 3D MOT. The 3D MOT on the D_2 line has a decay time of 23 sec. Adding the D_1 laser lowers decreases this time but a D_1 repump increases it back almost to the D_2 value. The data in panel a was taken with exposure time of 0.2 sec (b) SNR of detecting the number of atoms using the D_1 line vs. the camera exposure duration.

In conclusion, I have demonstrated the ability to load and control the micro-optical trap, and also to measure the number of atoms in it, reaching the single atom level. Most importantly, the knowledge and experience I gained working in the current setup is invaluable in designing the new setup which will be tailored towards the experiments in this proposal.

3.2 Sensitive RF spectroscopy

After building the 3D MOT for detecting the small number of atoms loaded into the micro trap, we realized we can use it also in rf spectroscopy - a measurement of the number of atoms out-coupled by the RF pulse versus its frequency. From this measurement, many physical observables can be obtained. One of them is the contact parameters, C, that measured the change in energy in respect to a change in the inverse of the scattering length. At high frequency, the contact interactions in 3D should give rise to a power-law scaling of the rf lineshape:$\Gamma(\nu) \rightarrow \frac{C}{2^{3/2}\pi^2}\nu^{-3/2}$, where ν is the RF frequency in unit of E_F/h and C is in unit of Nk_F, where N is the total number of atoms and k_F is the Fermi k-vector [29]. In previous works, rf signal could be measured only up to $\nu < 12$ $\mathrm{E_F}$, while the power law appears above 5 $\mathrm{E_F}$ [34]. We have developed a novel rf spectroscopy method that can detect the atoms out-coupled by the rf pulse in the MOT, thus providing the rf spectroscopy with single atoms level sensitivity. Using this method, we were able to measure signals up to 150 - $200E_F$, opening a new tool to calibrate the interaction parameters and directly measure the contact tail power law. I am an equal contributor of the paper summarizing our result, which was recently published in the arXiv and is currently under review [33].

4 Research plan

From the experience I gained during the last three years, and in particular during the work on loading the microtrap and detecting the number of atoms in it, it is clear to me that in order to successfully built the new platform, I need to build a dedicated apparatus which is tailored to this goal. In what follows I will explain what are the requirements from this new apparatus, and the experiments I wish to conduct after I build it.

4.1 New experimental apparatus

The following are the requirements from the new apparatus:

- **Fast data acquisition**.
  As described in Ref. [17], about 350 experiments were needed for each experimental value, e.g., a distance between the traps, the interaction, and the gate time. This number is typical in many ultracold atoms experiments, especially if the signal is weak since it originates from single atoms. However, the cooling and preparation stages in these experiments take a considerable time. For example: 3D MOT loading - 20–50 sec, Grey molasses cooling on the D1 line - 10msec, Magnetic evaporation - 20–30 sec, Optical evaporation - 3-5 sec. In our current apparatus, in which the preliminary results presented in chapter 3 were obtained, the preparation time is approximately 70 sec. Hence, including alignments and calibrations, a complete scan of 350 points will takes a working day. I this apparatus we are aiming at a shorter duration of approximately 8 sec per measurement. I believe this is feasible because we do not require the large number of atoms and deep quantum degeneracy obtained in the current setup. Short experimental cycle will also help in terms of magnetic field and laser stability.

- **Good vacuum separation between the atomic source chamber and the experimental chamber.**
  The atoms are released continually from a dispenser at a temperature of more than 300K in the first vacuum chamber. In this chamber, the atoms are collected, cooled and then sent through a nozzle to the main chamber. To detect a single atom in the main chamber, there cannot be atoms traveling around the microtraps area. This means we need to have excellent separation between the source and main chambers. This will be achieved by differential pumping between the source chamber and the rest of the system (geometrical separation). In addition, the use of a 2D MOT will enable dynamical control of the source, namely the ability to turn off completely the stream of atoms traveling to the main chamber. To summarize, the use of multiple chambers with differential pumping, and employing a 2D MOT as an atomic source will allow

high atoms flux and as the same time good vacuum separation and real-time control of the source.

- **High NA at least in one axis.**
  There are a number of reasons for the requirement to create a high NA at least on one axis. First, to load a single atom to a microtraps, an optical trap with ω_0 smaller than 1.8 μm is needed [32]. Second, for the detection, a small number of photons are scattered by a single atom, and many as possible need to be collected. Previous works obtained NA=0.86 working with an objective having NA=0.6 and a hemispheric lens on the optical viewport [27]. The working distance between the window and the objective was ~ 150 μm in these works. As a result, most of the other laser beams were coming at a total reflected angle relative to the vacuum window. Another group working with Caesium used an objective with NA=0.92 which was placed inside the vacuum chamber [37]. Both techniques reached high NA, but both set a major constraint on the system. Section 4.2 describes a new method to use an objective with NA=0.65 which meets our requirements. Our approach is to incorporate transverse beams that will help increase the axial trapping frequency in the microtrap. This will allow working with slightly lower NA without harming the performance of gates, etc. By working with a slightly lower NA, we will not have to place the objective inside the vacuum chamber or use an hemispheric lens.

- **Minimize background scattered photons.**
  The group's first apparatus uses a final ("science") chamber with a small optical windows (but with high NA from 3 axes, figure 2) and ,unfortunately, in spite of its anti-reflection coating has 5% optical reflection per surface. We suspect that overheating during the UHV baking caused the anti-reflection coating (AR) to be damaged. As a result, the scattered photons from the windows surfaces created a large background signal in the detection which hampered our effort to measure a single atoms at high fidelity. To avoid this problem in the new setup, one axis with high NA will be used, and all the other windows will be taken farther away from the atoms position. In addition, the vacuum system will be baked only up to 200° C in order to avoid damage to the AR coating.

- **Generating a stable magnetic field.**
  It is important that we will be able to control with high accuracy and stability the interaction between two spin states. As explained earlier, this is done by applying a uniform magnetic field in the position of the atoms. As shown in section 1.1.1, the magnetic field needed for the proposed system is approximately 202.14 ± 6.8 G (the non-interaction field is at 209G). Therefore, two coils at Helmholtz configuration are needed. The chamber geometry determines the coil parameters (radius, distance from

the atoms, number of threads, current). We will use the extensive experience we already have in our group in stabilizing the field to few parts-per-million (ppm).

By considering all these requirements, I have designed a new apparatus containing two chambers (see figure 7). The first chamber is similar to what we are already using successfully in our current working apparatus. At this chamber the atomic sources are mounted and 2D MOT is operating. The second chamber is where we will perform all cooling stages, and then continue do the actual experiments. The planned apparatus is a long glass chamber ("2D chamber") connected to an octagon stainless steel chamber ("experimental chamber"). The entire system will be baked to allow ultra-high vacuum ($\sim 10^{-11}$ torr). In addition, we plan to coat the experimental chamber by a non-evaporable getter (NEG) coating that effectively acts as a pump and reduce out-gassing. In the 2D chamber, ^{40}K atoms will be released from home-made dispenser which we already produced several years ago and are kept under vacuum since. The atoms will be collected and trapped by a 2D MOT that creates a stream of cold atoms. A laser beam in the third axis pushes the atoms through a nuzzle to the experimental chamber. The atoms are then collected and cooled in the experimental chamber by a 3D MOT. The 3D MOT consists of three counter-propagating circularly polarized beams with a retro-reflection configuration containing both cooling and repumping frequencies. The laser light at a wavelength of 767.7nm for the cooling and repump is generated from two DBR lasers with tapered amplifiers. Both lasers are offset-locked relative to a common master laser which is stabilized using saturated absorption spectroscopy ("master laser"). All these laser were already built, and we now need only to build the tapered amplifiers.

The temperature in 3D MOT is limited due to the Doppler limit $T_D = \frac{\hbar\Gamma}{2k_B}$ [22]. In ^{40}K, the Doppler limit is $T_D = 145\ \mu$K. Then, grey molasses cooling is used on the D_1 transition to lower the atom temperature to approximately $15\ \mu K$. For the D_1 cooling, another DBR laser with a tapered amplifier will be used. The laser is locked on the D_1 transition of the ^{39}K using saturated absorption spectroscopy (separated system from the D_2 transition locking system). The frequency is shifted ($\sim$705 MHz) to the cooling D1 transition in ^{40}K by using two Acousto-Optic-Modulatos (AOM). For the repump beam, a side-band is added to the laser by using a home-made, high-frequency, electro-optic-modulator (EOM). Hence, the cooling and repump are phase locked, which is necessary for the grey molasses cooling technique to work. Next,the atoms are loaded into an optical dipole trap created by two lasers of 50 W power and wavelength of 1064nm. These lasers have a waist of $\omega_0 = 250\ \mu$m and they cross at an angle of 14°, creating a $\sim 100\ \mu$K deep trap. To evaporate the atoms, the optical depth is lowered up to $T/T_F \approx 0.5$. Then, we will turn on the optical microtraps and load them. After loading, the crossed optical dipole trap will be shut off and and the power of the microtraps will be gradually reduced to spill out the atoms at the higher energy levels. At the final stage, a magnetic field gradient will be used to reach a single occupation at each trap [32].

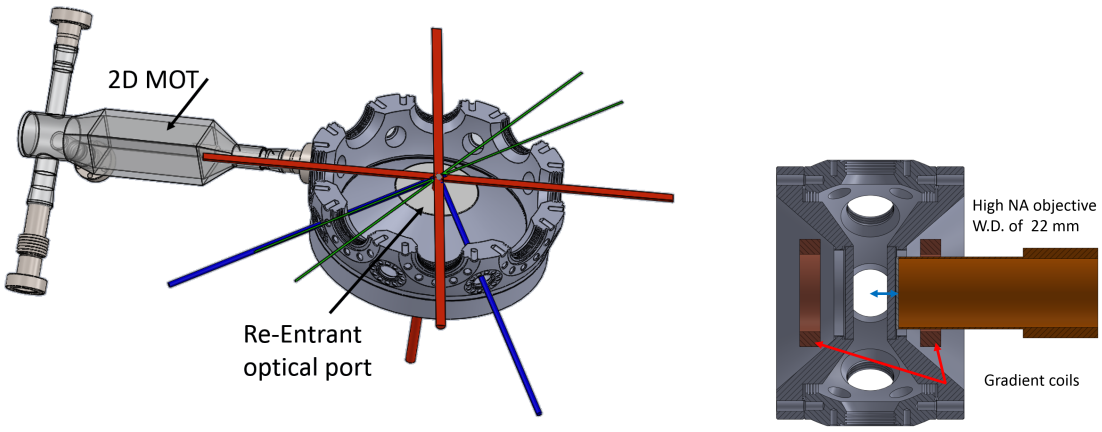

(a) **(b)**

Figure 7 – (a) A 3D model of the new apparatus. The atoms are captured in a 2D MOT and then sent to the experimental chamber, where they are caught by a 3D MOT (beams marked by red lines) and subsequently optically cooled in a grey molasses on the D_1 line. The crossed optical dipole trap is shown as green lines. The detection beams have an angle of 68° relative to the z-axis (blue lines). This angle is important to Raman side-band detection (see section 4.3). In the new apparatus, a working distance of approximately 22 mm is planned between the position of the atoms and the surface of the last viewport. (b) A cross-section view of the new apparatus. Two Helmholtz coils will be used both for generating the quadrupole field needed for the 3D MOT and the homogeneous field of the Feshbach resonance. A high NA objective with a working distance of 22 mm (blue arrow) is also shown.

4.2 Microtrap

As described in section 3.1.1, I have already built a microtrap in the working apparatus by using a home-built objective with NA=0.3. The numerical calculations of the $\sqrt{\text{SWAP}}$ gate showed that the NA must be large (>0.8) in order to obtain a short time scale for the gate. This is a result of the aspect ratio between the radial and the axial frequencies in a Gaussian beam. To achieve such a high NA, an objective must be designed with a hemispheric lens attached to the vacuum chamber or be placed inside the vacuum chamber. Both possibilities restrict the versatility of the apparatus. Instead, we propose a new scheme which overcomes

this problem even with NA as low as 0.65. The trap frequencies depended on the waist ω_0 in the radial direction and the Rayleigh range z_R in the longitudinal axis.

$$\nu_r \propto \frac{1}{\omega_0}, \qquad \nu_z \propto \frac{1}{z_R} \quad . \tag{19}$$

For given NA, the aspect ratio is given by NA$= \omega_0/z_R = \sqrt{2}\nu_z/\nu_r$, and as shown in figure 8, the aspect ratio can be less then 1.6 with NA$>$0.85. Alternatively, we propose to add a standing wave in the longitudinal axis. The 1D optical lattice can be matched to the microtrap radial frequency, giving an aspect ratio$\sim$ 1.32 (which equivalent to NA=1.1). The standing wave will be created by two laser beams at 90° degrees from the microtrap longitudinal axis and separated by $\sim 8°$, creating 2D "pancakes" with a distance of $\sim 7.64\,\mu$m between them. As shown in figure 8, the standing wave deepens the potential in the $\hat{z}$ axis and creates a large effective NA.

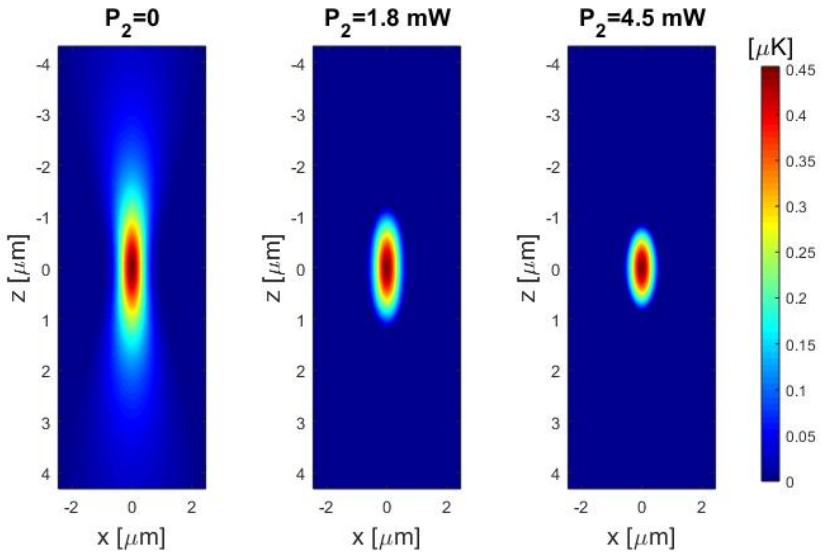

Figure 8 – Combined potential of the microtrap and optical lattice vs. the power in the optical lattice (P_2). The microtrap is created from an NA=0.65 and 2 μW. The optical lattice reduces the aspect ratio and yield an effective NA of 1.1 (right most graph).

4.3 Single atom detection

Detecting the presence, internal state, and position of a single atom in a microtrap is one of the major challenges in this project. In recent years, new techniques of detecting a single ^{40}K

atom have been reported [8, 31, 12]. A simple way to detect a single atom with high fidelity is to use 3D MOT, similar to what was presented in chapter 3. The key advantage of this technique over other detection schemes is the observation time and therefore the number of collected photons can be made almost arbitrarily large. As shown in figure 9a, the signal of a single ^6Li atom even with a low NA is distinguishable. In addition, as described in chapter 3, the signal in our system with ^{40}K atoms is approximately 2700 $\frac{photon}{atom \cdot sec}$. Ultimately, the detection duration is limited by the decay time of the MOT, which is determined by collisions with the background gas. However, this technique cannot obtain a spatially and spin state resolved detection. To address this problem, a spin state resolved detection can be added to the 3D MOT detection, as shown in [33]. This is done by encoding, with a microwave pulse, the state $|9/2, -7/2\rangle \rightarrow |7/2, -5/2\rangle$, which is magnetically trappable. Then a magnetic trap is opened and trapped only the $|9/2, -7/2\rangle$ state and releases the second state. After waiting some time, the 3D MOT beams are opened and detect only the spin selected state. There is a possibility to build a small volume MOT and shuttle the atoms to separately detect the atoms in different traps and achieve an effective spatial resolution. This method is effective in creating and characterizing our initial state while not requiring more lasers with different frequencies or a high-resolution objective.

To create a full detection tool for the quantum computation, a spatial resolution ability is needed to add to the detection scheme. In other alkali Fermium, the detection of a single atom can made on the cycling transition. As describe in Ref.[4],a fluorescence imaging of a single ^6Li atom is possible but with a spatial resolution of $\sim 5\ \mu$m. For this imaging method, the atomic sample can be illuminated from the side with two counter propagating laser beams. Then, the fluorescence photons can be captured with a high-resolution objective in the orthogonal axis (the same one that creates the microtraps). By inducing a high magnetic field, the spin states can be resolved. For example, in a field of 204G, the differences between the transitions $|-9/2, -9/2\rangle_{^2S_{1/2}} \rightarrow |11/2, -11/2\rangle_{^2P_{3/2}}$ and $|-9/2, -7/2\rangle_{^2S_{1/2}} \rightarrow |11/2, -9/2\rangle_{^2P_{3/2}}$ is $4\,\Gamma$ (~ 25 MHz). The number of photons per atom is ~ 60 photon/μs. To detect such low photon numbers, a camera with a high quantum efficiency is required. Furthermore, it is necessary that one photon creates a signal above the noise level. Consequently, an electron multiplying charged-coupled device (EMCCD) should be used. The previous work in this area with ^{40}K cannot detect a single atom with fluorescence imaging due to the $3D_{3/2}$ transition that creates an untrappable potential that causes heating and loss during the detection [8].

overcome the heating problem, Lawrence et al. suggested and created a new scheme that cooled the atom during the fluorescence imaging in ^{40}K [8]. They used a Raman sideband cooling that was first proposed by Wineland in 1995 [24]. By adding a magnetic field, the two Zeeman sub-levels are split such that the states $|F, m_f\rangle_n$ and $|F-1, m_f+1\rangle_{n-1}$ are degenerate (n represents the vibrational state index). Then, by using a Raman transition, the atom can be pumped from $|F, m_f\rangle_n \longrightarrow |F-1, m_f+1\rangle_{n-1}$. The cooling cycle is complete

by optically pumping the atom back to the initial state. To ensure that the atom pumps back to the initial state without changing its vibrational index, one needs to work in the Lamb-Dicke regime [10]. Using Raman sideband cooling, the number of atoms at each site can be detected due to their fluorescence without heating. The fluorescence rate for single atom is $\sim 800 - 1000$ photon/sec and can be measured with the EMCCD camera, as shown in figure 9b. However, this technique cannot distinguish between the spin states, and its experimental setup is complex (lasers in D_1 and D_2 transitions that include four different frequencies).

This technique can be generalized to be spin sensitive by translating the spin state to a spatial position [6]. In this work performed with ^6Li, of the lattice sites, adiabatically splits to a local double well potential. At the same time, a magnetic field, with a gradient $\frac{\partial B_z(x)}{\partial x}$, is implemented. The magnetic force at each state is different in sign and based on their magnetic moment. Therefore, the potential minima experienced by the two spin states of opposite magnetic moment causes a separation of the spins into the two different sites on the local double-well, as shown in figure 9c. This method can be applied by encoding one of our states, which have the same sign of the magnetic moment, to another site with opposite magnetic moment sign and translating the spin state to a position. This scheme can complete the detection method to a measure the position and spin states of a single ^{40}K atom.

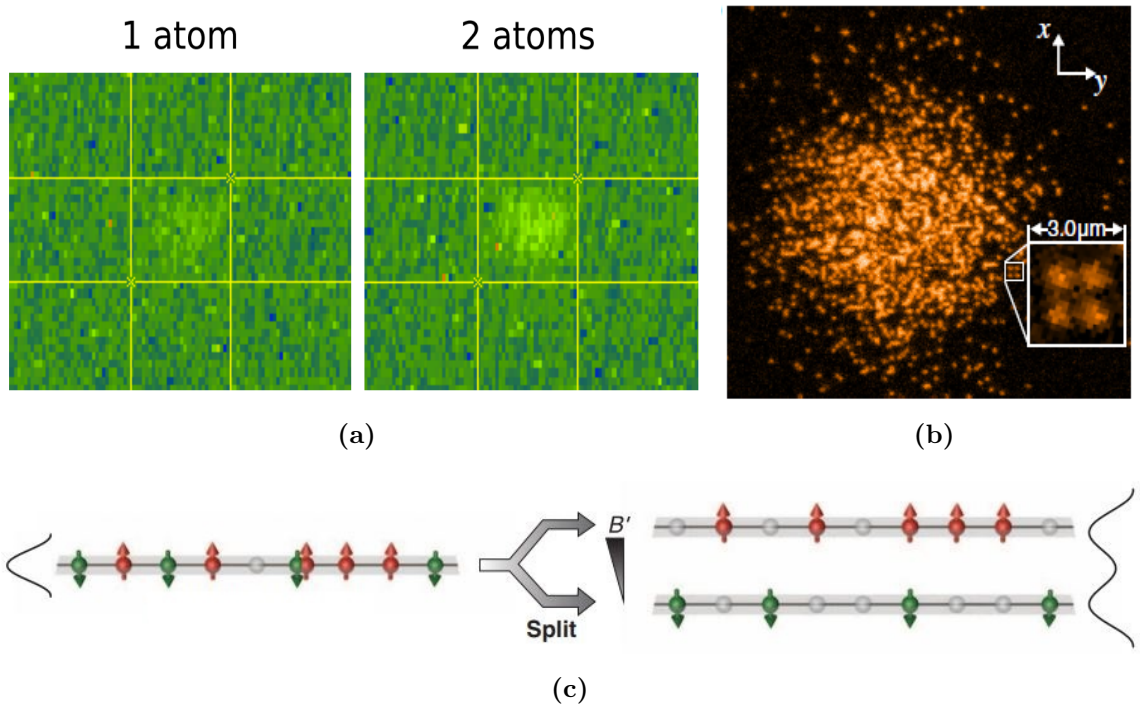

Figure 9 – Single atom detection. (a) A signal from a single atom and two atoms of ^6Li by using a 3D MOT. This picture was adopted from [36]. In this measurement, the photon was collected by lens with NA=0.17 and the exposure time was 0.5 sec. (b) A signal from a single ^{40}K atom in lattice with high resolution using a Raman sideband cooling technique. In this measurement, the signal per atom is ~ 1000 $\frac{\text{photon}}{\text{atom·sec}}$ was collected by a high NA objective, and the exposure time was 1 sec. This picture was adopted from [8]. (c) Schematic of the spin-resolved imaging. Each site was split based on the spin into a double-well potential by applying a magnetic field gradient. This picture was adopted from [6].

4.4 Single atom interferometer

The computational scheme is based on the ability to move microtraps without affecting the atomic state, including the phase between the two qubit states. In 1984, Sir M. Berry showed that a cyclic evolution of a wave-function acquires a phase shift that is the sum of a dynamical phase and a geometric phase [5]. The phases depend on the trajectory; therefore, each qubit may accumulate a different phase depending on the path. One goal of this research is to

find such trajectory to eliminate this phase difference. This work proposes a new sequence that includes the Ramsey interferometer technique and the split spin dependence technique. In the Ramsey interferometer technique, a first pulse of $\pi/2$ takes the initial state $|\downarrow\rangle$ into a superposition state $(|\downarrow\rangle + |\uparrow\rangle)/\sqrt{2}$. After a free evolution time of T, the second arbitrary pulse then recombines the atomic wave packets. Finally, the probability amplitude of the state $|\uparrow\rangle$ is given by [7, 28]

$$|\uparrow\rangle = \frac{1}{\sqrt{2}}\left(\cos\frac{\Omega\tau}{2}e^{-i(\omega_2 T-\phi_1)} + \sin\frac{\Omega\tau}{2}e^{-i(\omega_1 T-\phi_2)}\right) \tag{20}$$

where ϕ_i is the phase of the i Raman pulse, Ω and τ are the Rabi frequency and the pulse duration of the i Raman interactions respectively, and ω_1 and ω_2 are the perturbed frequencies of the two ground states. The population probability of the state $|\uparrow\rangle$ is written as

$$P_\uparrow = \frac{1}{2}\left\{1 + \sin(\Omega\tau)\cos\left[(\omega_2 - \omega_1)T + \Delta\phi\right]\right\} \tag{21}$$

As shown in section 4.3, the superposition state can be split after the first $\pi/2$ pulse by using the split spin dependently technique. As a result, the spin state can be mapped to a position and the state involved to $1/\sqrt{2}\,(|\downarrow\rangle_0 \otimes |\uparrow\rangle_1)$. A movement of a single microtrap relative to the second adds a phase to the first microtrap, $\left(e^{-i\theta}|\downarrow\rangle_0 \otimes |\uparrow\rangle_1\right)/\sqrt{2}$. Afterwards, the two microtrap combined together (the inverse operation of the split spin technique) and another $\pi/2$ pulse combines the atomic wave packet.

$$|\psi'\rangle = \frac{1}{2}\left(e^{-i\theta}\left[|\downarrow\rangle_0 + |\uparrow\rangle_0\right] + \left[|\uparrow\rangle_0 - |\downarrow\rangle_0\right]\right) \tag{22}$$

The probability to measured the atom in $|\uparrow\rangle$ state is given by

$$P_\uparrow = \frac{1}{2}\left\{1 + \sin(\Omega\tau)\cos\left[(\omega_2 - \omega_1)T + \Delta\phi + \theta\right]\right\} \tag{23}$$

As shown in figure 10b,the probability $P_\uparrow$, without a relative phase between the two paths can be measured as a function of the waiting duration T as reference. Then, a relative phase can be added to one of the states by changing the position of the first microtrap, $d(t)$, relative to the second microtrap and measuring the phase between this measurement and the reference measurement.

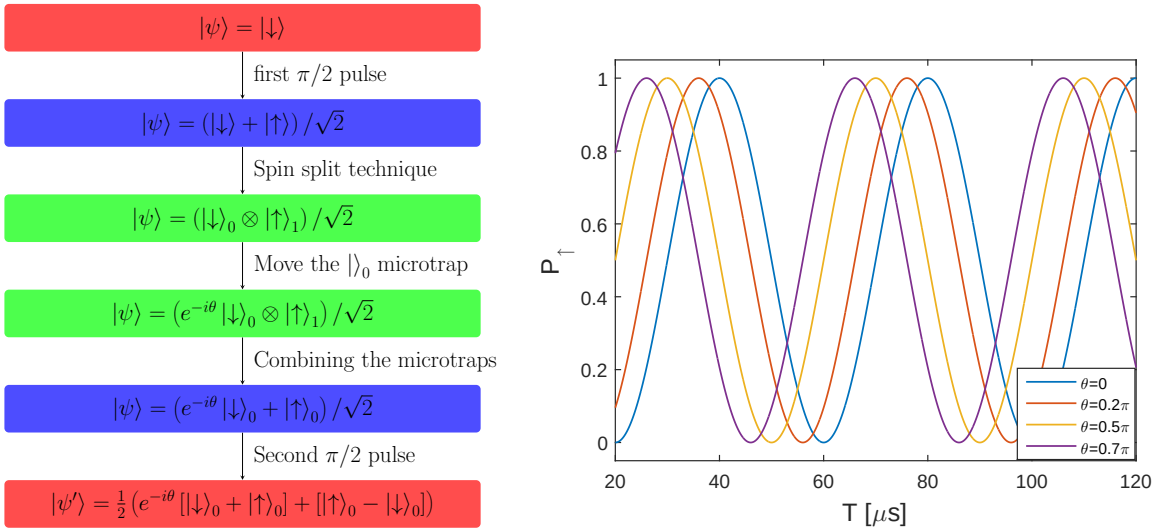

Figure 10 – (a) The single atom interferometer flowchart. (b) Plot of equation 23 for several phases θ.

4.5 $\sqrt{\text{SWAP}}$ gate

The main goal of this work is to apply a two-qubit gate in an apparatus of ultracold atoms. AS explained in section 2.3.2, the gate parameters are deteriorated by the tunneling energy. We measured this parameter as a function of the distance between the microtrap. The system prepares with a single atom in one microtrap microtrap is empty. Then, after a duration of τ, the second microtrap is detected. In this measurment, the spin and position do not need to be detected; therefore, 3D MOT detection can be used. After the tunneling duration is measured, the $\sqrt{\text{SWAP}}$ gate duration and the interaction energy U are determinate, as shown in equation 14. The experimentally $\sqrt{\text{SWAP}}$ gate error is described by the density matrix after the two qubits gate $\rho_{\sqrt{\text{SWAP}}}$, that is given by

$$\begin{bmatrix} 1 & 0 & 0 & 0 \\ 0 & \frac{1}{2}(1+i) & \frac{1}{2}(1-i) & 0 \\ 0 & \frac{1}{2}(1-i) & \frac{1}{2}(1+i) & 0 \\ 0 & 0 & 0 & 1 \end{bmatrix} . \tag{24}$$

In general case, ρ can be expanded into a superpostion $\rho = \sum_i \lambda_i A_i$ of mutually orthogonal Hermitian operators A_i, to form a basis and obey the equation $Tr(A_i A_j) = 4\delta_{ij}$[13]. For a two-qubits system, a convenient set of operators is given by the sixteen operators $\sigma_i^{(1)} \otimes \sigma_j^{(2)}$, where $i, j = 0, 1, 2, 3$, and $\sigma_i^{(k)}$ is a Pauli matrix in $\hat{i}$ axis of qubit k [30]. The density matrix

can be reconstructed by measurement of the expectation values $\left\langle \sigma_i^{(1)} \otimes \sigma_j^{(2)} \right\rangle$. The measurement project the quantum state into one state $|x_1 \otimes x_2\rangle$where $x_i \in \{0, 1\}$. By repeatedly preparing and measuring the final quantum state, the average population in states $|x_1 \otimes x_2\rangle$ is obtained to calculate the expectation values of $\sigma_z^{(1)}$, $\sigma_z^{(2)}$, and $\left\langle \sigma_z^{(1)} \otimes \sigma_z^{(2)} \right\rangle$. To measure the operators that involve σ_y and σ_x, the eigenvectors can map the eigenvectors of σ_z with the following unitary transformation

$$\sigma_z = U_{y,x} \sigma_{y,x} U_{y,x}^{-1} \tag{25}$$

where U_x and U_y are some unitary rotation of a single qubit gate on the Bloch sphere. To obtain all sixteen expectation values, nine different settings must be used. The fidelity F of the reconstructed state can be determinate by $F = \langle\psi| \rho_\psi |\psi\rangle$. This parameter is influenced from the gate parameters (U, gate duration and the tunneling duration) and from noise in the system. The $\sqrt{\text{SWAP}}$ gate parameters is then scanned with the demand of high fidelity $F > 0.99$.

5 Summary

In conclusion, I suggest a new method of quantum computation in an ultracold fermionic system. This method requires a number of an experimental tools that can create a single atom in a microtrap, detect a single atom with spatial discrimination and spin-resolved, and control the in site interaction and the tunneling interaction. I described our new apparatus which is set up in these days. We want to measure and characterize a two new method. The first method applies a Stern Gerlach interferometer of a single atom. This method can give us a spatial distinction of the qubits. The second method creates a new platform for quantum computation and to realize a two-qubit gate with high fidelity.

References

[1] L Allen and JH Eberly Optical Resonance. Two-level atoms dover publications inc. *New York*, 1987.

[2] Rami Barends, Julian Kelly, Anthony Megrant, Andrzej Veitia, Daniel Sank, Evan Jeffrey, Ted C White, Josh Mutus, Austin G Fowler, Brooks Campbell, et al. Superconducting quantum circuits at the surface code threshold for fault tolerance. *Nature*, 508(7497):500–503, 2014.

[3] Daniel Barredo, Sylvain De Léséleuc, Vincent Lienhard, Thierry Lahaye, and Antoine Browaeys. An atom-by-atom assembler of defect-free arbitrary two-dimensional atomic arrays. *Science*, 354(6315):1021–1023, 2016.

[4] JHW Becher. *Towards Spin and Site-Resolved, Single-Atom Imaging of 6Li Atoms in a Multiwell Potential*. PhD thesis, Master thesis, Heidelberg University, 2016.

[5] Michael V Berry. Quantal phase factors accompanying adiabatic changes. *Proceedings of the Royal Society of London. A. Mathematical and Physical Sciences*, 392(1802):45–57, 1984.

[6] Martin Boll, Timon A Hilker, Guillaume Salomon, Ahmed Omran, Jacopo Nespolo, Lode Pollet, Immanuel Bloch, and Christian Gross. Spin-and density-resolved microscopy of antiferromagnetic correlations in fermi-hubbard chains. *Science*, 353(6305):1257–1260, 2016.

[7] Ch J Bordé, Ch Salomon, S Avrillier, A Van Lerberghe, Ch Bréant, D Bassi, and G Scoles. Optical ramsey fringes with traveling waves. *Physical Review A*, 30(4):1836, 1984.

[8] Lawrence W Cheuk, Matthew A Nichols, Melih Okan, Thomas Gersdorf, Vinay V Ramasesh, Waseem S Bakr, Thomas Lompe, and Martin W Zwierlein. Quantum-gas microscope for fermionic atoms. *Physical review letters*, 114(19):193001, 2015.

[9] Juan I Cirac and Peter Zoller. Quantum computations with cold trapped ions. *Physical review letters*, 74(20):4091, 1995.

[10] Robert H Dicke. Coherence in spontaneous radiation processes. *Physical Review*, 93(1):99, 1954.

[11] David P DiVincenzo et al. The physical implementation of quantum computation. *arXiv preprint quant-ph/0002077*, 2000.

[12] GJA Edge, R Anderson, D Jervis, DC McKay, R Day, S Trotzky, and JH Thywissen. Imaging and addressing of individual fermionic atoms in an optical lattice. *Physical Review A*, 92(6):063406, 2015.

[13] Ugo Fano. Description of states in quantum mechanics by density matrix and operator techniques. *Reviews of Modern Physics*, 29(1):74, 1957.

[14] Richard P Feynman. Simulating physics with computers. *International journal of theoretical physics*, 21(6):467–488, 1982.

[15] Rudolf Grimm, Matthias Weidemüller, and Yurii B Ovchinnikov. Optical dipole traps for neutral atoms. *Advances in atomic, molecular, and optical physics*, 42:95–170, 2000.

[16] David Hayes, Paul S Julienne, and Ivan H Deutsch. Quantum logic via the exchange blockade in ultracold collisions. *Physical review letters*, 98(7):070501, 2007.

[17] Jonathan P Home, David Hanneke, John D Jost, Jason M Amini, Dietrich Leibfried, and David J Wineland. Complete methods set for scalable ion trap quantum information processing. *Science*, 325(5945):1227–1230, 2009.

[18] John Hubbard. Electron correlations in narrow energy bands. In *Proceedings of the Royal Society of London A: Mathematical, Physical and Engineering Sciences*, volume 276, pages 238–257. The Royal Society, 1963.

[19] A Imamog, David D Awschalom, Guido Burkard, David P DiVincenzo, Daniel Loss, M Sherwin, A Small, et al. Quantum information processing using quantum dot spins and cavity qed. *Physical Review Letters*, 83(20):4204, 1999.

[20] Stefan Kuhr et al. *A controlled quantum system of individual neutral atoms*. PhD thesis, Universitäts-und Landesbibliothek Bonn, 2003.

[21] Brian J Lester, Niclas Luick, Adam M Kaufman, Collin M Reynolds, and Cindy A Regal. Rapid production of uniformly filled arrays of neutral atoms. *Physical review letters*, 115(7):073003, 2015.

[22] VS Letokhov, VG Minogin, and BD Pavlik. Cooling and capture of atoms and molecules by a resonant light field. *Soviet Journal of Experimental and Theoretical Physics*, 45:698, 1977.

[23] Daniel Loss and David P DiVincenzo. Quantum computation with quantum dots. *Physical Review A*, 57(1):120, 1998.

[24] Ch Monroe, DM Meekhof, BE King, SR Jefferts, WM Itano, DJ Wineland, and P Gould. Resolved-sideband raman cooling of a bound atom to the 3d zero-point energy. *Physical Review Letters*, 75(22):4011, 1995.

[25] Michael A Nielsen and Isaac L Chuang. *Quantum computation and Quantum information*. Cambridge University Press India, 2000.

[26] Jeremy L O'Brien. Optical quantum computing. *Science*, 318(5856):1567–1570, 2007.

[27] Maxwell F. Parsons, Florian Huber, Anton Mazurenko, Christie S. Chiu, Widagdo Setiawan, Katherine Wooley-Brown, Sebastian Blatt, and Markus Greiner. Site-resolved imaging of fermionic ^{6}Li in an optical lattice. *Phys. Rev. Lett.*, 114:213002, May 2015.

[28] Norman F Ramsey. A molecular beam resonance method with separated oscillating fields. *Physical Review*, 78(6):695, 1950.

[29] Mohit Randeria, W Zwerger, and M Zwierlein. The bcs–bec crossover and the unitary fermi gas. In *The BCS-BEC Crossover and the Unitary Fermi Gas*, pages 1–32. Springer, 2012.

[30] CF Roos, GPT Lancaster, M Riebe, H Häffner, W Hänsel, S Gulde, C Becher, J Eschner, F Schmidt-Kaler, and R Blatt. Bell states of atoms with ultralong lifetimes and their tomographic state analysis. *Physical review letters*, 92(22):220402, 2004.

[31] Friedhelm Serwane, Gerhard Zürn, Thomas Lompe, TB Ottenstein, AN Wenz, and S Jochim. Deterministic preparation of a tunable few-fermion system. *Science*, 332(6027):336–338, 2011.

[32] Friedhelm Serwane, Gerhard Zürn, Thomas Lompe, TB Ottenstein, AN Wenz, and S Jochim. Deterministic preparation of a tunable few-fermion system. *Science*, 332(6027):336–338, 2011.

[33] Constantine Shkedrov, Yanay Florshaim, Gal Ness, Andrey Gandman, and Yoav Sagi. High sensitivity rf spectroscopy of a strongly-interacting fermi gas. *arXiv preprint arXiv:1803.01770*, 2018.

[34] JT Stewart, JP Gaebler, TE Drake, and DS Jin. Verification of universal relations in a strongly interacting fermi gas. *Physical Review Letters*, 104(23):235301, 2010.

[35] Christof Weitenberg, Stefan Kuhr, Klaus Mølmer, and Jacob F Sherson. Quantum computation architecture using optical tweezers. *Physical Review A*, 84(3):032322, 2011.

[36] Andre Niklas Wenz. *From Few to Many: Ultracold Atoms in Reduced Dimensions*. PhD thesis, 2013.

[37] Ryuta Yamamoto, Jun Kobayashi, Takuma Kuno, Kohei Kato, and Yoshiro Takahashi. An ytterbium quantum gas microscope with narrow-line laser cooling. *New Journal of Physics*, 18(2):023016, 2016.